Spectral line shape in the limit of frequent velocity-changing collisions

Nikodem Stolarczyk,* Piotr Wcisło, and Roman Ciuryło

Institute of Physics, Faculty of Physics, Astronomy and Informatics,
Nicolaus Copernicus University in Toruń, ul Grudziądzka 5, 87-100 Toruń, Poland

(Dated: March 28, 2024)

The speed-dependent spectral line profiles collapse into a simple Lorentz profile in the regime dominated by the velocity-changing collisions. We derive general formulas for the effective width and shift of the Lorentzian for arbitrary speed-dependent collisional broadening and shift and velocity-changing collision operators. For a quadratic speed dependence of collisional broadening and shift, and the billiard ball model of velocity-changing collisions, we provide simple analytical expressions for the effective Lorentzian width and shift. We show that the effective Lorentzian width and shift split into components originating from the well-known Dicke-narrowed Doppler width, speed-averaged collisional broadening and shift, their speed dependencies, and a product term that mixes the contributions of the broadening and shift speed dependencies. We show how the components depend on rates of speed-changing and velocity-changing collisions related to the perturber/absorber mass ratio. We validate analytical formulas numerically on the example of H_2 transition perturbed by He.

Keywords: molecular line shapes, inhomogeneous broadening and shift, velocity-changing collisions, Dicke narrowing

I. INTRODUCTION

The shape of molecular spectral line affected by Doppler broadening and absorber-perturber collisions, in the general case, requires numerical evaluation and cannot be represented by a simple analytical function, unless some simplifications or assumptions are made [1]. The goal of this work is to show that, in the case when the velocity-changing collisions dominate other line-shape effects, the spectral line shape collapses to an ordinary Lorentz profile and the expressions for its width and shift can be provided analytically.

The Lorentz profile has been used for over a century to describe collisionally-broadened atomic and molecular spectral lines. It is particularly justified at high pressure of perturbers, much lighter than absorbers, in microwave spectral range, where the speed dependence of collisional broadening and shift [2, 3], as well as Doppler broadening, can be neglected. Interestingly, also the Gaussian shape of the spectral line can collapse to the Lorentz profile when the velocity-changing collisions reduce the mean free path of the absorber well below the wavelength of absorbed radiation as predicted by Dicke [4, 5] in the fifties. It was later demonstrated numerically [6], that the weighted sum of Lorentz profiles (WSL) [7, 8], under frequent velocity-changing collisions described by the billiard-ball model [9, 10] approaches the Lorentz profile and the convergence is faster for lower perturber/absorber mass ratio. It is related to relative contribution of speed change during velocity-changing collisions which is determined by perturber/absorber mass ratio [11, 12]. Recently, studies on line shapes for which width is dominated by the speed-dependent collisional shift led to formulating a simple an-

alytical expression [13, 14] (see Eq. (15) in Ref. [13]) for width of Lorentzian profile approximating such line shape when speed-dependent collisional shift is described by a quadratic function [15] and velocity-changing collisions are approximated by the hard-collision model [16, 17]. The phenomenological finding from Ref. [13] got justification in a derivation [18] coming from the speed-dependent hard-collision profile [19, 20].

In this article, we generalize the results from Ref. [18]; we derive general formulas for the effective width and shift of a Lorentzian to which a sophisticated line shape model, based on any arbitrary speed-dependent collisional broadening and shift and velocity-changing collision operator, converges in the limit of frequent velocity-changing collisions. For quadratic speed dependencies of collisional width and shift, and the billiard ball model of velocity-changing collisions, we provide a simple analytical expression for the effective Lorentzian width and shift. We show how their components depend on rates of speed-changing and velocity-changing collisions related to the perturber/absorber mass ratio. We validate the analytical formulas numerically.

II. ALGEBRAIC REPRESENTATION OF A SPECTRAL LINE SHAPE

In general, the shape of an isolated spectral line affected by Doppler broadening and collisions with perturbers can be evaluated [21, 22] from a function $h(\omega, \vec{v})$,

$$I(\omega) = \frac{1}{\pi} \text{Re} \left\{ (1, h(\omega, \vec{v})) \right\}, \qquad (1)$$

where $(\cdot, \cdot)$ is defined as a product $(a(\vec{v}), b(\vec{v})) = \int d^3\vec{v} f_{m_A}(\vec{v}) a(\vec{v}) b(\vec{v})$ of two functions $a(\vec{v})$, $b(\vec{v})$ of absorber velocity $\vec{v}$, $f_{m_A}(\vec{v}) = (\pi v_{m_A}^2)^{-3/2} \exp(-v^2/v_{m_A}^2)$ is Maxwellian distribution, $v_{m_A} = \sqrt{k_B T/(2m_A)}$ is

---
* NikodemStolarczyk319@gmail.com

the most probable speed of the absorber having mass m_A at temperature T, and k_B is Boltzmann's constant. Function $h(\omega, \vec{v})$ fulfils transport-relaxation kinetic equation [22],

$$1 = -i(\omega - \omega_0 - \vec{k} \cdot \vec{v})h(\omega, \vec{v}) - \hat{S}^f h(\omega, \vec{v}), \quad (2)$$

where ω_0 is unperturbed transition frequency, $\vec{k}$ is a wavevector of radiation, and operator $\hat{S}^f$ describes the effect of collisions with perturbers.

Equations (1) and (2) can be converted into an algebraic form expanding function $h(\omega, \vec{v})$,

$$h(\omega, \vec{v}) = \sum_{s=0}^{\infty} c_s(\omega)\varphi_s(\vec{v}), \quad (3)$$

in a set of orthonormal functions fulfilling condition $(\varphi_s(\vec{v}), \varphi_{s'}(\vec{v})) = \delta_{s,s'}$. We set $\varphi_0(\vec{v}) = 1$. The expansion coefficients $c_s(\omega)$ depend only on frequency for given operator $\hat{S}^f$. In this basis, any operator $\hat{A}$ can be represented by matrix $\mathbf{A}$, having matrix elements $[\mathbf{A}]_{s,s'} = (\varphi_s(\vec{v}), \hat{A}\varphi_{s'}(\vec{v}))$.

The shape of an isolated spectral line can have algebraic representation by a series of Lorentz profiles. Following the approaches from [10, 21, 23, 24] and notation described in Refs. [6, 22, 25], the line shape can be written as [6, 25, 26]:

$$I(\omega) = \frac{1}{\pi}\text{Re}\left\{c_0(\omega)\right\}, \quad (4)$$

where the coefficient $c_0(\omega)$ can be evaluated by solving a set of complex linear equations,

$$\underline{\mathbf{b}} = \mathbf{L}(\omega)\underline{\mathbf{c}}(\omega), \quad (5)$$

for the coefficients $c_s(\omega)$, where $s = 0, 1, ..., s_{\max}$. Here the column $\underline{\mathbf{b}}$ contains unity in the position 0 and zeros in other positions, i.e. $[\underline{\mathbf{b}}]_s = \delta_{0,s}$, and the column $\underline{\mathbf{c}}(\omega)$ consists of the coefficients $c_s(\omega)$, i.e. $[\underline{\mathbf{c}}(\omega)]_s = c_s(\omega)$. The matrix $\mathbf{L}(\omega)$ depends on the frequency ω and has the following form:

$$\mathbf{L}(\omega) = -i(\omega - \omega_0)\mathbf{1} + i\mathbf{K} - \mathbf{S}^f, \quad (6)$$

where ω_0 corresponds to the unperturbed frequency of the transition, $\mathbf{1}$ is the unit matrix, $[\mathbf{1}]_{s,s'} = \delta_{s,s'}$, $\mathbf{K}$ is the matrix that represents the Doppler shift, $\mathbf{S}^f = \mathbf{S}_D^f + \mathbf{S}_{VC}^f$ is the matrix which represents the collision operator split into two components: $\mathbf{S}_D^f$ is the matrix which represents the "dephasing and relaxation" [27, 28] collisional width and shift and $\mathbf{S}_{VC}^f$ is the matrix which represents the "velocity-changing" collision operator also affected by dephasing and relaxation. The representation used here has a property $[\mathbf{S}_{VC}^f]_{s,0} = [\mathbf{S}_{VC}^f]_{0,s} = 0$ for any s and $[\mathbf{K}]_{0,0} = 0$. Moreover, all matrices discussed in this work are symmetric.

In practice, the coefficient $c_0(\omega)$ is calculated using the diagonalization technique (c.f. [24, 29, 30]). To do it in this way, one needs to find the full set of eigenvectors, $\underline{\mathbf{e}}_j$, and corresponding eigenvalues ε_j which fulfill the following equation:

$$(i\mathbf{K} - \mathbf{S}^f)\underline{\mathbf{e}}_j = \varepsilon_j\underline{\mathbf{e}}_j, \quad (7)$$

where $j = 0, 1, ..., s_{\max}$. Once the eigenvectors and eigenvalues are known, the coefficient $c_0(\omega)$ can be computed from the following expression:

$$c_0(\omega) = \sum_{j=0}^{s_{\max}} \frac{\beta_j[\underline{\mathbf{e}}_j]_0}{\varepsilon_j - i(\omega - \omega_0)}, \quad (8)$$

where the coefficients β_j fulfill the relation $\underline{\mathbf{b}} = \sum_{j=0}^{s_{\max}} \beta_j\underline{\mathbf{e}}_j$. The main advantage of this approach is that the time-consuming diagonalization can be carried out once and this is sufficient to calculate the whole line shape.

III. HIGH FREQUENCY OF THE VELOCITY-CHANGING COLLISIONS LIMIT

Our derivation is carried out in the limit where the velocity-changing collisions dominate over the Doppler broadening and collisional broadening and shift. We assume the absolute values of all matrix elements of $\mathbf{K}$ and $\mathbf{S}_D^f$, as well as detuning, $\omega - \omega_0$, to be much smaller than the absolute value of the effective optical frequency of velocity changing collisions, ν_{opt}. Importantly, ν_{opt} can be complex due to the dephasing associated with optical velocity-changing collisions. All nonzero matrix elements of $\mathbf{S}_{VC}^f$ are directly proportional to ν_{opt}. The recognition of ν_{opt} as a complex quantity was originally put forth by Rautian and Sobelmann [17]. Subsequent support for this notion came from the comparison between measurements [31] and theoretical estimations [32]. The complex form of ν_{opt} has been justified through both semiclassical approaches [17, 33–35] and quantum treatments [33, 36–41], see also the references cited therein.

For the matrix $\mathbf{S}_{VC}^f$ we can calculate eigenvectors, $\underline{\mathbf{e}}_j^{VC}$, and eigenvalues, ε_j^{VC}, which fulfil the following equation:

$$-\mathbf{S}_{VC}^f\underline{\mathbf{e}}_j^{VC} = \varepsilon_j^{VC}\underline{\mathbf{e}}_j^{VC}. \quad (9)$$

It is easy to see that one of the eigenvectors of the matrix having property $[\mathbf{S}_{VC}^f]_{s,0} = [\mathbf{S}_{VC}^f]_{0,s} = 0$ is vector $\underline{\mathbf{b}}$ and its corresponding eigenvalue is zero. Therefore, we can set $\underline{\mathbf{e}}_0^{VC} = \underline{\mathbf{b}}$ and $\varepsilon_0^{VC} = 0$. Consequently, for $j \neq 0$ we have $[\underline{\mathbf{e}}_j^{VC}]_0 = 0$ and $\varepsilon_j^{VC} \sim \nu_{\text{opt}}$.

Now we can rewrite Eq. (7) in the form:

$$(-\mathbf{S}_{VC}^f - \mathbf{S}_D^f + i\mathbf{K})\underline{\mathbf{e}}_j = \varepsilon_j\underline{\mathbf{e}}_j, \quad (10)$$

where the matrix, which we want to diagonalize, is split into the dominating part $\mathbf{S}_{VC}^f$ and the perturbation part containing $\mathbf{S}_D^f$ and $\mathbf{K}$. We take advantage of that and

approximate eigenvectors $\underline{\mathbf{e}}_j$ by $\underline{\mathbf{e}}_j^{VC}$ and eigenvalues ε_j by ε_j^{VC} and improve them by perturbation corrections. Setting $\underline{\mathbf{e}}_j \approx \underline{\mathbf{e}}_j^{VC}$ we get $\beta_j = \delta_{j,0}$. In this, way Eq. (8) can be approximated with the Lorentz profile:

$$c_0(\omega) \approx \frac{1}{\varepsilon_0 - i(\omega - \omega_0)}, \qquad (11)$$

where the eigenvalue ε_0 is approximated by second-order perturbation. The eigenvalues, ε_j, in the second-order perturbation are given by the following expression:

$$\varepsilon_j \approx \varepsilon_j^{VC} + \sum_{s,s'=0}^{s_{\max}} [\underline{\mathbf{e}}_j^{VC}]_s (-[\mathbf{S}_D^f]_{s,s'} + i[\mathbf{K}]_{s,s'})[\underline{\mathbf{e}}_j^{VC}]_{s'} +$$
$$+ \sum_{\substack{j'=0 \\ j' \neq j}}^{s_{\max}} \frac{(\sum_{s,s'=0}^{s_{\max}} [\underline{\mathbf{e}}_j^{VC}]_s (-[\mathbf{S}_D^f]_{s,s'} + i[\mathbf{K}]_{s,s'})[\underline{\mathbf{e}}_{j'}^{VC}]_{s'})^2}{\varepsilon_j^{VC} - \varepsilon_{j'}^{VC}}.$$
$$(12)$$

This equation for ε_0 simplifies to the following form

$$\varepsilon_0 \approx -[\mathbf{S}_D^f]_{0,0} +$$
$$+ \sum_{j'=1}^{s_{\max}} \frac{\{\sum_{s'=1}^{s_{\max}} (-[\mathbf{S}_D^f]_{0,s'} + i[\mathbf{K}]_{0,s'})[\underline{\mathbf{e}}_{j'}^{VC}]_{s'}\}^2}{-\varepsilon_{j'}^{VC}}, \quad (13)$$

remembering that $\varepsilon_0^{VC} = 0$, $[\underline{\mathbf{e}}_0^{VC}]_s = \delta_{0,s}$ and $[\mathbf{K}]_{0,0} = 0$. In this way, we get a single Lorentz profile,

$$I(\omega) = \frac{1}{\pi} \frac{\Gamma_{\mathrm{eff}}}{\Gamma_{\mathrm{eff}}^2 + (\omega - \omega_0 - \Delta_{\mathrm{eff}})^2}, \qquad (14)$$

in the limit of frequent velocity-changing collisions, here

$$\Gamma_{\mathrm{eff}} + i\Delta_{\mathrm{eff}} = \varepsilon_0. \qquad (15)$$

It should be noted that we can always use the basis in which matrix $\mathbf{S}_{VC}^f$ is diagonal. In such case $[\underline{\mathbf{e}}_j^{VC}]_s = \delta_{j,s}$, $\varepsilon_j^{VC} = -[\mathbf{S}_{VC}^f]_{j,j}$ and Eq. (13) takes simple form

$$\varepsilon_0 \approx -[\mathbf{S}_D^f]_{0,0} + \sum_{s=1}^{s_{\max}} \frac{(-[\mathbf{S}_D^f]_{0,s} + i[\mathbf{K}]_{0,s})^2}{[\mathbf{S}_{VC}^f]_{s,s}}. \qquad (16)$$

Furthermore, one can use a basis in which if a matrix element is nonzero, $[\mathbf{S}_D^f]_{0,s} \neq 0$, then the corresponding matrix element is zero, $[\mathbf{K}]_{0,s} = 0$, and, if $[\mathbf{K}]_{0,s} \neq 0$ then $[\mathbf{S}_D^f]_{0,s} = 0$. It is a simple consequence of the symmetry of the corresponding operators. The collisional broadening and shift depend on the absolute value of the absorber velocity, $v = |\vec{v}|$, and are not dependent on velocity direction. On the other hand, the Doppler shift is proportional to the scalar product $\vec{k} \cdot \vec{v}$ which depends on velocity direction. Taking this into account, we can rewrite Eq. (16) in the following form:

$$\varepsilon_0 \approx -[\mathbf{S}_D^f]_{0,0} - \sum_{s=1}^{s_{\max}} \frac{[\mathbf{K}]_{0,s}^2}{[\mathbf{S}_{VC}^f]_{s,s}} + \sum_{s=1}^{s_{\max}} \frac{[\mathbf{S}_D^f]_{0,s}^2}{[\mathbf{S}_{VC}^f]_{s,s}}. \qquad (17)$$

IV. APPLICATION IN CASE OF QUADRATIC SPEED-DEPENDENT COLLISIONAL BROADENING AND SHIFT

To get physical insight into the expressions derived above, we consider matrix representation using Burnett functions [9] described in Appendix A. We assume quadratic speed dependence of collisional broadening and shift [15]. It means that the operator

$$\hat{S}_D^f = -\Gamma(v) - i\Delta(v) \qquad (18)$$

is determined by $\Gamma(v)$ and $\Delta(v)$ given in the following form

$$\Gamma(v) + i\Delta(v) = \Gamma_0 + i\Delta_0 + (\Gamma_2 + i\Delta_2)\left(\frac{v^2}{v_m^2} - \frac{3}{2}\right), \qquad (19)$$

where Γ_0 and Δ_0 are the collisional broadening and shift parameters, averaged over absorber velocity, respectively. Quadratic speed dependencies of collisional broadening and shift are described by Γ_2 and Δ_2 parameters, respectively.

Discussing the velocity-changing collisions, we will focus on the case where matrix $\mathbf{S}_{VC}^f$ is diagonal or is approximated by a diagonal matrix.

In the Burnett functions basis representation, instead of the index $s = 0, 1, ..., s_{\max}$, we prefer to use two other indices, $n = 0, 1, ..., n_{\max}$ and $l = 0, 1, ..., l_{\max}$. The pair of indices nl can be connected with $s = n + (n_{\max} + 1)l$ and $s_{\max} = n_{\max} + (n_{\max} + 1)l_{\max}$.

The properties of matrix elements in Burnett functions representation are summarized in Appendix A. The assumptions made above constrain the number of nonzero matrix elements which contribute to Eq. (17) to only a few,

$$\varepsilon_0 = -[\mathbf{S}_D^f]_{00,00} - \frac{[\mathbf{K}]_{00,01}^2}{[\mathbf{S}_{VC}^f]_{01,01}} + \frac{[\mathbf{S}_D^f]_{00,10}^2}{[\mathbf{S}_{VC}^f]_{10,10}}. \qquad (20)$$

Now we can explicitly express the matrix elements: $[\mathbf{K}]_{00,01} = \omega_D\sqrt{1/2}$, where $\omega_D = kv_{m_A}$, $[\mathbf{S}_D^f]_{00,00} = -(\Gamma_0 + i\Delta_0)$, and $[\mathbf{S}_D^f]_{00,10} = -(\Gamma_2 + i\Delta_2)\sqrt{3/2}$.

A. Hard collision model

To discuss the velocity-changing collisions we first consider the hard collision (HC) model [16, 17], discussed recently in Ref. [18] in a similar context. The HC model is frequently used due to its simplicity, despite its shortcomings. In many situations, it helps to get some analytical results. The operator $\hat{S}_{HC}^f$ describing hard velocity changing collisions has the following form:

$$\hat{S}_{HC}^f h(\omega, \vec{v}) = -\nu_{\mathrm{opt}} h(\omega, \vec{v}) + \nu_{\mathrm{opt}} \int d^3\vec{v}' f_{m_A}(\vec{v}') h(\omega, \vec{v}'), \qquad (21)$$

where ν_{opt} is the effective optical frequency of velocity-changing collisions, which, in the general case, can be a complex number [17, 31, 32, 36]. It can be shown that in any orthonormal base assuming $\varphi_0(\vec{v}) = 1$, the matrix representation of the $\hat{S}^f_{HC}$ operator is diagonal, $[\mathbf{S}^f_{HC}]_{s,s'} = -\nu_{\text{opt}}\delta_{s,s'}(1-\delta_{0,s})$. All its diagonal elements are equal to $-\nu_{\text{opt}}$, except $[\mathbf{S}^f_{HC}]_{0,0} = 0$. Therefore, also in the Burnett functions representation, we can write that $[\mathbf{S}^f_{HC}]_{01,01} = [\mathbf{S}^f_{HC}]_{10,10} = -\nu_{\text{opt}}$. Inserting these matrix elements into Eqs. (20) and (15) we got

$$\Gamma^{HC}_{\text{eff}} + i\Delta^{HC}_{\text{eff}} = \Gamma_0 + i\Delta_0 + \frac{\omega_D^2}{2\nu_{\text{opt}}} - \frac{3\Gamma_2^2}{2\nu_{\text{opt}}} + \frac{3\Delta_2^2}{2\nu_{\text{opt}}} - i\frac{3\Gamma_2\Delta_2}{\nu_{\text{opt}}}. \tag{22}$$

The above result has also been obtained in our recent paper with a different method, see Eqs. (19a)–(19d) in Ref. [18], where we have shown that speed-dependent hard-collision profile [20] collapses into a simple Lorentz profile in the limit of frequent velocity-changing collisions.

B. Soft collision model

In the case when perturbers are much lighter then absorbers, the velocity changing collisions are described by soft collision (SC) model [42]. This model was introduced by Galatry [43] into the theory of Dicke narrowed spectral line shapes. By that time, the Galatry profile (GP) became one of the most frequently used expression to describe collisionally-narrowed spectra. The exact speed-dependent Galatry profile (SDGP) with quadratic speed dependence of collisional width and shift was given in Ref. [44] and should be not confused with its approximated expression provided by Prime et al [45] using approach from Ref. [46]. It was shown in Refs. [9, 10] that the velocity changing soft collisions operator $\hat{S}^f_{HC}$ is represented with a diagonal matrix operator in the Burnett functions basis. The relevant matrix elements are given by the following expressions: $[\mathbf{S}^f_{SC}]_{00,00} = 0$, $[\mathbf{S}^f_{SC}]_{01,01} = -\nu_{\text{opt}}$, $[\mathbf{S}^f_{SC}]_{10,10} = -2\nu_{\text{opt}}$, see Refs. [9, 10]. In contrast to the HC model, the matrix elements $[\mathbf{S}^f_{SC}]_{01,01}$ and $[\mathbf{S}^f_{SC}]_{10,10}$ are not identical. Inserting these matrix elements into Eqs. (20) and (15) yields:

$$\Gamma^{SC}_{\text{eff}} + i\Delta^{SC}_{\text{eff}} =$$
$$\Gamma_0 + i\Delta_0 + \frac{\omega_D^2}{2\nu_{\text{opt}}} - \frac{3\Gamma_2^2}{4\nu_{\text{opt}}} + \frac{3\Delta_2^2}{4\nu_{\text{opt}}} - i\frac{3\Gamma_2\Delta_2}{2\nu_{\text{opt}}}. \tag{23}$$

The three last terms of this equation are two times smaller then the ones derived in case of the HC model, Eq. (22) [18].

C. Billiard ball model

The billiard ball (BB) model [10] provides a more realistic description of the velocity-changing collisions. This model properly accounts for the perturber/absorber mass ratio, $\alpha = m_p/m_a$. The matrix describing such velocity-changing collisions $[\mathbf{S}^f_{BB}]_{nl,n'l'} = \nu_{\text{opt}}f_D M^{E*}_{nl,n'l'}$ is determined by coefficients $M^{E*}_{nl,n'l'}$ [9, 10] defined in Appendix A. This matrix is diagonal and the factor $f_D = 1$ in case of $\alpha = 0$, which corresponds to the soft collision (SC) model. For nonzero α, the matrix $[\mathbf{S}^f_{BB}]_{nl,n'l'}$ is not diagonal and f_D becomes greater than one, reaching $32/(9\pi) \approx 1.132$ for $\alpha = \infty$ [10]. Nevertheless, we can approximate the original matrix by its diagonal simplification with the same diagonal elements $[\mathbf{S}^f_{BB}]_{nl,nl}$. The coefficients $M^{E*}_{01,01} = -1$ and $M^{E*}_{10,10} = -2M_1$, where $M_1 = m_A/(m_A + m_B)$ are of our particular interest since these allow to provide the explicit form of the matrix elements $[\mathbf{S}^f_{BB}]_{01,01} = -\nu_{\text{opt}}f_D$ and $[\mathbf{S}^f_{BB}]_{10,10} = -\nu_{\text{opt}}f_D 2/(1 + \alpha)$. In contrast to the HC model, these matrix elements are not identical. The matrix element $[\mathbf{S}^f_{BB}]_{01,01} \approx \nu_{\vec{v}}$ describes relaxation rate, $\nu_{\vec{v}}$, of the velocity vector, $\vec{v}$. On the other hand, $[\mathbf{S}^f_{BB}]_{10,10} \approx \nu_{v^2}$ describes relaxation rate, ν_{v^2}, of v^2 which is directly related to speed, v. As it was shown in Refs. [12, 47], the ratio between the speed, v- or its square, v^2-changing collisions and velocity, $\vec{v}$-changing collisions rate $\nu_{v^2}/\nu_{\vec{v}} = [\mathbf{S}^f_{BB}]_{10,10}/[\mathbf{S}^f_{BB}]_{01,01} = 2/(1+\alpha)$ varies with α. This ratio agrees well with results obtained from the classical molecular dynamics simulations based on realistic molecular interaction potentials [11, 47]. Inserting the matrix elements $[\mathbf{S}^f_{BB}]_{01,01}$ and $[\mathbf{S}^f_{BB}]_{10,10}$ into Eqs. (20) and (15) we got

$$\Gamma^{BB}_{\text{eff}} + i\Delta^{BB}_{\text{eff}} = \Gamma_0 + i\Delta_0 + \frac{\omega_D^2}{2\nu_{\vec{v}}} - \frac{3\Gamma_2^2}{2\nu_{v^2}} + \frac{3\Delta_2^2}{2\nu_{v^2}} - i\frac{3\Gamma_2\Delta_2}{\nu_{v^2}}. \tag{24}$$

We do not need to limit our discussion to the diagonal approximation in this place. We can take into account the full matrix, $[\mathbf{S}^f_{BB}]_{nl,nl}$, and use Eq. (13). However, to derive the exact analytical expressions, we used another method described in Appendix B, where we found that $\nu_{\vec{v}} = \nu_{\text{opt}}$, $\nu_{v^2} = \nu_{\text{opt}}(2/(1 + \alpha))(f_D/f_{v^2})$, and got the following

$$\Gamma^{BB}_{\text{eff}} + i\Delta^{BB}_{\text{eff}} = \Gamma_0 + i\Delta_0 + \frac{\omega_D^2}{2\nu_{\text{opt}}} +$$
$$\left(-\frac{3\Gamma_2^2}{2\nu_{\text{opt}}} + \frac{3\Delta_2^2}{2\nu_{\text{opt}}} - i\frac{3\Gamma_2\Delta_2}{\nu_{\text{opt}}}\right)\frac{1+\alpha}{2}\frac{f_{v^2}}{f_D}. \tag{25}$$

Γ^{BB}_{eff} and $i\Delta^{BB}_{\text{eff}}$ are the effective width and shift of the Lorentzian, which the quadratic speed-dependent billiard ball profile (SDBBP) [6] collapses to, under frequent velocity-changing collisions. This expression is a generalization of Eq. (22) [18] to the arbitrary mass ratio α case. It should be noted that the factor f_{v^2}/f_D (except

TABLE I. Coefficients f_D, f_{v^2} and their ratio f_D/f_{v^2} evaluated for different α within billiard ball model.

α	f_D	f_{v^2}	f_D/f_{v^2}
0	1	1	1
1/100	1.00000331561954	1.00000991995975	0.99999339572530
1/50	1.00001319212471	1.00003935941918	0.99997383373542
1/20	1.00008114950708	1.00023998438455	0.99984120323127
1/10	1.00031613831745	1.00091992503335	0.99939676821212
1/5	1.00119948726834	1.00336387252056	0.99784287105456
1/4	1.00182496341562	1.00501525070746	0.99682563295473
1/3	1.00310178272716	1.00822551613664	0.99491806810334
1/2	1.00636139570140	1.01565719613513	0.99084750202223
2/3	1.01027159637697	1.02349086931942	0.98708413202431
1	1.01895378488101	1.03806540223391	0.98158919725889
3/2	1.03178515946401	1.05522030753985	0.97779122718887
2	1.04294734723661	1.06757150938264	0.97693441429486
3	1.05994565861	1.0835515889	0.9782142996
4	1.0717514674	1.093265697	0.980321134
5	1.08028126	1.09975074	0.982296461
10	1.101660	1.114423	0.9885474
20	1.11523	1.122707	0.99334
50	1.12464	1.1280	0.997
100	1.1280	1.1280	1
∞	$32/9\pi \approx 1.131$	1.131	1

$\alpha = 0$ and $\alpha = \infty$ for which is equal to one), is slightly greater than unity but not more than 2.36% in the worst case of $\alpha = 2$, see Table I.

Equations (22) and (25) become equivalent when $\alpha = 1$ and corresponding $f_{v^2}/f_D = 1.018756$ is approximated by unity. Some equivalence of the HC model and BB model with $\alpha = 1$ was already discussed in Ref. [6, 12, 47]. For $\alpha = 0$ and the corresponding $f_{v^2}/f_D = 1$, it means in case of SC [42, 43], Eq. (25) provides the effective width and shift of Lorentzian to which quadratic speed-dependent Galatry profile [6, 44] collapses under frequent velocity-changing collisions. In this case Eq. (25) is reduced to Eq. (23). It is worth mentioning that comparing the asymptotic behavior of hard and soft collision models we can see that the components of the effective width and shift related to suppressed Doppler effect [4] and thermally-averaged collisional broadening and shift are the same for both models. In contrast, the components related to the speed dependence of collisional broadening and shift are two times smaller in the case of the soft collision model. It is a natural consequence of the fact that $\nu_{v^2}^{SC} = 2\nu_{v^2}^{HC}$, when we keep the same $\nu_{\vec{v}}^{SC} = \nu_{\vec{v}}^{HC}$ for both models.

V. COMPONENTS OF EFFECTIVE WIDTH AND SHIFT

In line with our previous paper [18], it is important to note that the Dicke parameter can take on complex values, $\nu_{\text{opt}} = \nu_{\text{opt}}^r + i\nu_{\text{opt}}^i$ [17, 31, 32, 36]. Therefore, we can decompose the effective Lorentzian width and shift of the asymptotic quadratic correlated speed-dependent billiard ball profile [6, 25, 27, 48] into several contributions:

$$\Gamma_{\text{eff}} = \Gamma_0 + \Gamma_\gamma + \Gamma_\delta + \Gamma_{\gamma\delta} + \Gamma_{\omega_D}, \tag{26a}$$

$$\Delta_{\text{eff}} = \Delta_0 + \Delta_\gamma + \Delta_\delta + \Delta_{\gamma\delta} + \Delta_{\omega_D}. \tag{26b}$$

Assuming quadratic speed-dependent collisional broadening and shift as well as velocity-changing collisions described by the billiard ball model, these contributions are:

$$\Gamma_\gamma = -\frac{f_{v^2}}{f_D}\frac{1+\alpha}{2}\frac{\nu_{\text{opt}}^r}{|\nu_{\text{opt}}|^2}\frac{3}{2}\Gamma_2^2, \tag{27a}$$

$$\Gamma_\delta = \frac{f_{v^2}}{f_D}\frac{1+\alpha}{2}\frac{\nu_{\text{opt}}^r}{|\nu_{\text{opt}}|^2}\frac{3}{2}\Delta_2^2, \tag{27b}$$

$$\Gamma_{\gamma\delta} = -2\frac{f_{v^2}}{f_D}\frac{1+\alpha}{2}\frac{\nu_{\text{opt}}^i}{|\nu_{\text{opt}}|^2}\frac{3}{2}\Gamma_2\Delta_2, \tag{27c}$$

$$\Gamma_{\omega_D} = \frac{\nu_{\text{opt}}^r}{|\nu_{\text{opt}}|^2}\frac{1}{2}\omega_D^2, \tag{27d}$$

$$\Delta_\gamma = \frac{f_{v^2}}{f_D}\frac{1+\alpha}{2}\frac{\nu_{\text{opt}}^i}{|\nu_{\text{opt}}|^2}\frac{3}{2}\Gamma_2^2, \tag{27e}$$

$$\Delta_\delta = -\frac{f_{v^2}}{f_D}\frac{1+\alpha}{2}\frac{\nu_{\text{opt}}^i}{|\nu_{\text{opt}}|^2}\frac{3}{2}\Delta_2^2, \tag{27f}$$

$$\Delta_{\gamma\delta} = -2\frac{f_{v^2}}{f_D}\frac{1+\alpha}{2}\frac{\nu_{\text{opt}}^r}{|\nu_{\text{opt}}|^2}\frac{3}{2}\Gamma_2\Delta_2, \tag{27g}$$

$$\Delta_{\omega_D} = -\frac{\nu_{\text{opt}}^i}{|\nu_{\text{opt}}|^2}\frac{1}{2}\omega_D^2. \qquad (27h)$$

For real $\nu_{\text{opt}} = \nu_{\text{opt}}^r$ ($\nu_{\text{opt}}^i = 0$) the components of effective width are: Γ_{ω_D} Γ_0, Γ_γ, Γ_δ. The first two terms represent collisionally-suppressed Doppler broadening and velocity-averaged collisional width, respectively. Γ_γ can be seen as a reduction of line width caused by the speed-dependence of collisional broadening. It is qualitatively coherent with findings in the other context of the speed-dependent Voigt profile (SDVP) [2, 3], where also the narrowing of the spectral line was triggered by speed-dependence of collisional broadening. On the other hand, Γ_δ represents an additional broadening of the line caused by the speed-dependent spread of collisional shift [7, 8, 49]. The character of these contributions does not depend on the sign of Γ_2 and Δ_2 parameters. The effective shift, in such circumstances, has only two components, Δ_0 and $\Delta_{\gamma\delta}$. The first one represents an ordinary velocity-averaged collisional shift, however, the second term is less obvious and is related to the product of speed dependencies of collisional broadening and shift or their correlation [18].

The other contributions, namely $\Gamma_{\gamma\delta}$, Δ_γ, Δ_δ, and Δ_{ω_D}, only come into play if ν_{opt} has a nonzero imaginary component, i.e., $\nu_{\text{opt}}^i \neq 0$. While we will not delve into a detailed discussion of these contributions, we will touch on the last one, Δ_{ω_D}. This shift arises due to Dicke-suppressed Doppler broadening, and it should decrease inversely with pressure, similar to the well-known Γ_{ω_D} [4]. This is because ν_{opt} is proportional to pressure, while ω_D remains constant at a given temperature. Therefore, in a moderate range of pressures, this term can potentially impact the precise determination of the line position. In fact, as we demonstrate in the following section, under certain conditions, Δ_{ω_D} can contribute up to 2 MHz to the effective line shift, Δ_{eff}.

To describe the relative contribution of each effect ($x = \gamma$, δ, $\gamma\delta$ or ω_D) under specific physical conditions, we introduce dimensionless parameters Γ_x/Γ_0 and Δ_x/Δ_0. It is worth noting that all collisional parameters, including ν_{opt}, Γ_0, Γ_2, Δ_0, and Δ_2, are proportional to gas pressure. Therefore, the dimensionless parameters Γ_x/Γ_0 and Δ_x/Δ_0 for $x = \gamma$, δ, and $\gamma\delta$ are independent of pressure. In fact, as we show in the following section, under certain conditions, Γ_δ can account for approximately 35% of Γ_0, and the absolute value of $\Delta_{\gamma\delta}$ can reach 5% of Δ_0 or 20% of Γ_0. For further details, please refer to the next section.

VI. NUMERICAL VALIDATION

We validated the analytical expressions obtained in the previous section. To achieve this, we compared our results with the numerical half width at half maximum (HWHM) Γ_{exact} and the frequency Δ_{exact} corresponding to the position of the maximum of the quadratic speed-
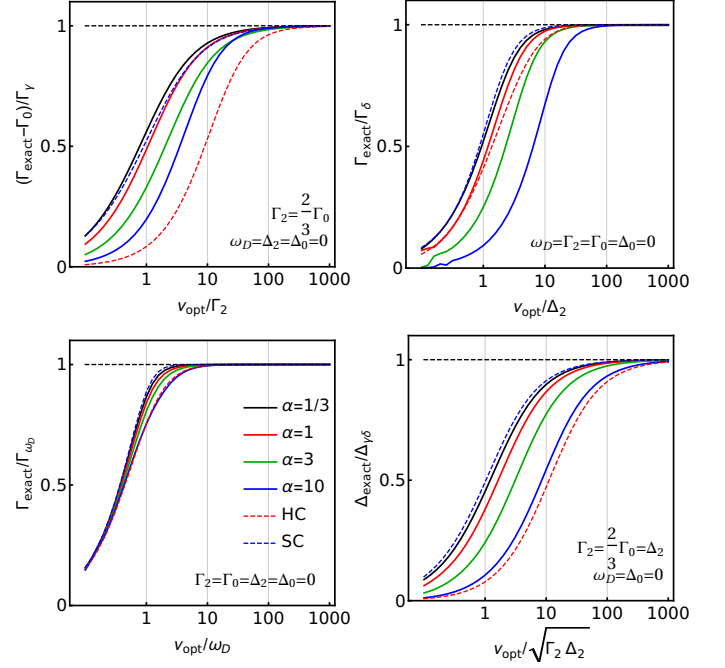
FIG. 1. Numerical verification of asymptotic formulas for Γ_γ, Γ_δ, Γ_{ω_D}, and $\Delta_{\gamma\delta}$. Panels (a)-(c) show ratios of $\Gamma_{\text{exact}}/\Gamma_\gamma$, $\Gamma_{\text{exact}}/\Gamma_\delta$, $\Gamma_{\text{exact}}/\Gamma_{\omega_D}$ as functions of $\nu_{\text{opt}}/\Gamma_2$, $\nu_{\text{opt}}/\Delta_2$, $\nu_{\text{opt}}/\omega_D$, respectively, where Γ_{exact} is numerically evaluated half width at half maximum (HWHM) of the quadratic speed-dependent billiard ball profile. Panel (d) shows the ratio of $\Delta_{\text{exact}}/\Delta_{\gamma\delta}$ as a function of $\nu_{\text{opt}}/\sqrt{\Gamma_2\Delta_2}$ where Δ_{exact} is numerically evaluated frequency corresponding to a maximum of the quadratic speed-dependent billiard ball profile. Presented ratios were evaluated for $\alpha = 1/3$, 1, 3, 10 as well as for $\alpha = 0$ it means soft collisions (SC) and hard collisions (HC).

dependent billiard ball profile [6]. Specifically, we focused on validating the formulas for Γ_γ, Γ_δ, Γ_{ω_D}, and $\Delta_{\gamma\delta}$ given by Eqs. (27a), (27b), (27d), and (27g), respectively. To carry out our calculations, we considered four values of $\alpha = 1/3, 1, 3, 10$, assuming real $\nu_{\text{opt}} = \nu_{\text{opt}}^r$, $\nu_{\text{opt}}^i = 0$.

To provide further insight, we also compared our results with those obtained from the soft collision model, which corresponds to the billiard ball model with $\alpha = 0$ and the speed-dependent Galatry profile [44] and the hard collision model [16, 17] which we discuss in detail in Ref. [18]. To simplify our analysis, we focused on one effect at a time and set the appropriate values for the line shape parameters: Γ_0, Δ_0, Γ_2, Δ_2, ω_D, ν_{opt} in the quadratic SDBBP.

Our results, shown in Fig. 1, demonstrate that Γ_{exact} converges to Γ_γ, Γ_δ, Γ_{ω_D} as well as Δ_{exact} approaches $\Delta_{\gamma\delta}$ in the limit of high ν_{opt}. However, we observed that the convergence is slower for higher values of α in the case of Γ_γ, Γ_δ, and $\Delta_{\gamma\delta}$. This observation is directly related to the fact that ν_{v^2} decreases with increasing α, while $\nu_{\vec{v}}$ remains constant. On the other hand, the situation is different for Γ_{ω_D}, which is determined by $\nu_{\vec{v}}$ and

is not dependent on α. As shown in Fig.1(c), the variations for α are weak in this case. However, for extremely large values of α, significant discrepancies for different α are observed. This topic has been discussed in detail in Ref. [6].

The discussion of the effective broadening component Γ_δ, which arises from the speed dependence of the collisional shift $\Delta(v)$, is important in this context. As mentioned earlier, an increase in α results in a decrease in ν_{v^2}. Therefore, we anticipate that, with other parameters held constant, an increase in α will result in an increase in Γ_δ. In the frequent velocity-changing collisions regime, where ν_{opt} dominates, an asymptotic analytical relation for quadratic SDBBP [6] can be written as:

$$\frac{\Gamma_\delta(\alpha)}{\Gamma_\delta(\alpha=0)} = \frac{f_{v^2}}{f_D}(1+\alpha) \approx 1+\alpha. \quad (28)$$

To simplify the calculation, the factor f_{v^2}/f_D in the asymptotic relation can be approximated as unity, introducing an error of less than 2%. We verified the accuracy of this approximation for finite values of $\nu_{\mathrm{opt}}/\Delta_2$ by simulating quadratic SDBBP for various values of $\nu_{\mathrm{opt}}/\Delta_2$ and α, while setting all other parameters (Γ_0, Δ_0, Γ_2, ν_{opt}^i, and ω_D) to zero. We then calculated Γ_{exact} for the simulated profiles, and plotted the ratios $\Gamma_{\mathrm{exact}}(\alpha)/\Gamma_{\mathrm{exact}}(\alpha=0)$ as a function of α for several values of $\nu_{\mathrm{opt}}/\Delta_2$ (3, 10, 100, 1000) in Fig.2. As shown in this figure, for $\nu_{\mathrm{opt}}/\Delta_2 = 10$, the simulation results are reproduced by Eq.(28) for small to moderate values of α up to $\alpha = 3$.

As mentioned in Section III, our derivation was conducted under the assumption that velocity-changing collisions dominate over both Doppler broadening and collisional broadening and shift, particularly their speed-dependent parts. To satisfy this condition, the interactions between the absorber and perturber molecules at the initial and final molecular states need to be either identical or closely similar [17, 33–41]. Physically, this requirement can be met in the case of rovibronic transitions
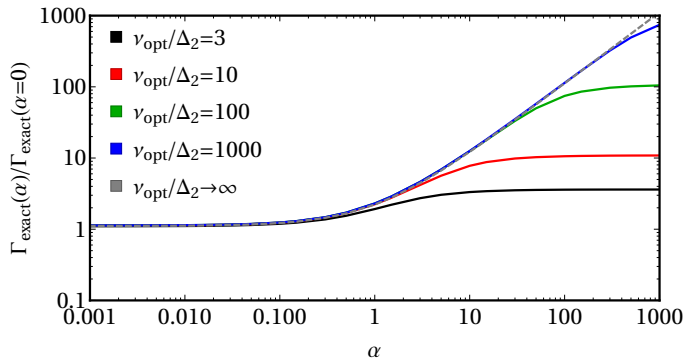

FIG. 2. Ratio of $\Gamma_{\mathrm{exact}}(\alpha)/\Gamma_{\mathrm{exact}}(\alpha=0)$ evaluated for several values ν_{opt}/Δ_2 within quadratic speed-dependent billiard ball profile in which parameters Γ_0, Δ_0, Γ_2, ν_{opt}^i, and ω_D were set to zero and its comparison with ratio $\Gamma_\delta(\alpha)/\Gamma_\delta(\alpha=0) \approx 1+\alpha$ obtained for $\nu_{\mathrm{opt}}/\Delta_2 \to \infty$.

TABLE II. Comparison of the Lorentz profile effective parameters for Q(1) 1-0 transition in H_2 perturbed by He ($\alpha = 2$) at 10 atm and 296 K obtained with Eqs. (27a)-(27h) derived from the billiard ball model (BB) and effective parameters from Ref. [18, 50] derived from hard collision model (HC). The line-shape parameters are $\Gamma_0 = 22.346$, $\Delta_0 = 90.971$, $\Gamma_2 = 10.856$, $\Delta_2 = 38.192$, $\nu_{\mathrm{opt}}^r = 404.148$, $\nu_{\mathrm{opt}}^i = -54.697$, $\omega_D = 21.659$ [50] are given in the units of 10^{-3} cm^{-1}.

Γ_x	$\Gamma_x^{BB}(10^{-3}$ cm$^{-1})$	Γ_x^{BB}/Γ_0	$\Gamma_x^{HC}(10^{-3}$ cm$^{-1})$	Γ_x^{HC}/Γ_0
Γ_0	22.346	1.000	22.346	1.000
Γ_γ	-0.645	-0.029	-0.430	-0.019
Γ_δ	7.974	0.357	5.316	0.238
$\Gamma_{\gamma\delta}$	0.613	0.027	0.409	0.018
Γ_{ω_D}	0.572	0.026	0.572	0.026
Γ_{eff}	30.860	1.381	28.215	1.263
Γ_{exact}	30.140	1.349	27.388	1.226

Δ_x	$\Delta_x^{BB}(10^{-3}$ cm$^{-1})$	Δ_x^{BB}/Δ_0	$\Delta_x^{HC}(10^{-3}$ cm$^{-1})$	Δ_x^{HC}/Δ_0
Δ_0	90.971	1.000	90.971	1.000
Δ_γ	-0.087	0.001	-0.058	-0.0006
Δ_δ	1.079	0.012	0.719	0.008
$\Delta_{\gamma\delta}$	-4.533	-0.050	-3.022	-0.033
Δ_{ω_D}	0.077	0.0008	0.077	0.0008
Δ_{eff}	87.507	0.962	88.688	0.975
Δ_{exact}	86.270	0.948	88.005	0.967

in molecular hydrogen. This can be observed through *ab initio* calculations, as presented in Ref. [50]. Additionally, it has been demonstrated in Refs. [28, 51] that such calculations, along with the use of SDBBP [6], can achieve sub percent agreement with experimental data.

It is seen from Fig. 1 that for $\alpha \leq 3$ and $\nu_{\mathrm{opt}}/\Gamma_2 \geq 10$ the error introduced by our approximation of Γ_γ does not exceed 16%. Similarly, for $\nu_{\mathrm{opt}}/\Delta_2 \geq 10$ our approximation of Γ_δ reproduces the corresponding width with inaccuracy less than 7%. Ultimately, if $\nu_{\mathrm{opt}}/\omega_D \geq 10$ the error on Γ_{ω_D} is at most 0.3%, which is significantly smaller than in the previous cases. On the other hand, for the pressure shift, if $\nu_{\mathrm{opt}}/\sqrt{\Gamma_2\Delta_2} \geq 10$ our approximation of $\Delta_{\gamma\delta}$ introduces error, which does not exceed 23%. In conditions where the speed-averaged values Γ_0 and Δ_0 are significantly greater than their speed dependencies, Γ_2 and Δ_2, the combined errors originating from these contributions result in a significantly smaller relative error on the entire line profile. Additionally, if the ν_{opt} dominates over the other line shape parameters (i.e., Γ_2, Δ_2, ω_D) by several dozens, our approximation should reproduce the original profile with several percent accuracy.

We compared the collapsed Lorentz profile to the SDBBP [6]. To do this, we examined the Q(1) 1-0 transition in H_2 perturbed by He at a pressure of 10 atm and a temperature of 296 K. We used the same line-shape parameters as in Ref. [18], which were obtained from Ref. [50]. The values of the line shape parameters can be found in the caption of Tab. II. This table lists all contributions Γ_x and Δ_x to the effective Lorentzian width Γ_{eff} and shift Δ_{eff}, respectively. These values were

calculated using Eqs. (27a)-(27h) under the assumption of a billiard ball model ($\alpha = 2$) for velocity-changing collisions and the hard collision model, as described in Ref. [18]. In Tab. II and Fig. 3, we used the unit of wave numbers $\widetilde{\nu} = 2\pi\omega/c$ instead of circular frequencies ω, which is more common in molecular spectroscopy for line shape parameters.

The ratios $\nu_{\mathrm{opt}}^{r}/\omega_D = 18.7$, $\nu_{\mathrm{opt}}^{r}/\Gamma_2 = 37.2$, and $\nu_{\mathrm{opt}}^{r}/\Delta_2 = 10.6$ demonstrate that our assumption from Sec. III, that the velocity-changing collisions dominate over Doppler broadening and collisional broadening and shift, is valid for the chosen conditions (pressure, temperature, molecular system). It is important to note that the values of Γ_0 and Δ_0 are not relevant in this context, as they only result in a simple convolution with the Lorentz profile determined by these parameters, which are additive in the case of Lorentz profiles. Furthermore, we have verified that the binary collision approximation holds well under these conditions, and the contribution of three-body collisions to collisional width and shift should not exceed the percentage level. For a detailed discussion, see Section II.B3 in Ref. [1].

The H_2 spectral line perturbed by He, for which $\alpha = 2$, allows us to observe the importance of the perturber/absorber mass ratio for the collapse of the spectral
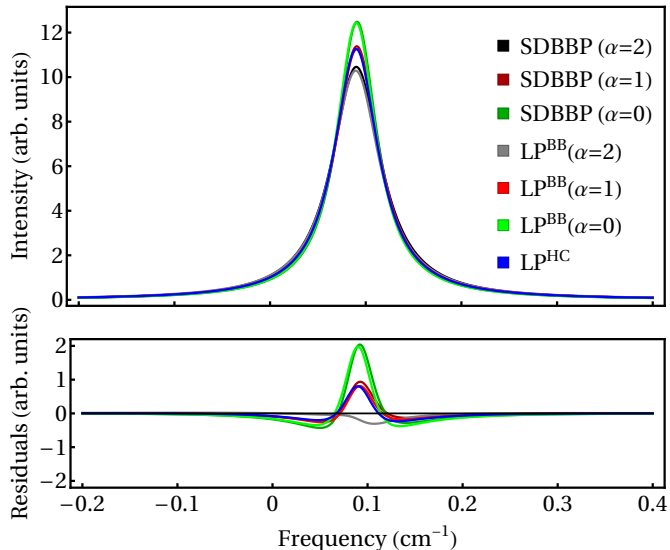

FIG. 3. A comparison of the reference speed-dependent billiard ball profiles (SDBBP) calculated with $\alpha = 2$, 1, 0 and parameters listed in the caption of Tab. II for Q(1) 1-0 transition in H_2 perturbed by He at 10 atm and 296 K [18, 50] and Lorentz profiles (LP^{BB}) derived as the collapsed SDBBP calculated with parameters given in this work by Eqs. (26a)-(27h) as well as Lorentz profile (LP^{HC}) derived as the collapsed hard collision profile from Ref. [18]. The area under each line is normalized to 1. The lower graph presents the residuals against reference SDBBP ($\alpha = 2$) having α corresponding to H_2-He system with the same color notation as in the upper panel.

line shape to a Lorentz profile due to frequent velocity-changing collisions. As shown in Tab. II, the use of the BB model results in a Lorentz profile that is 9.4% wider than the profile obtained from the HC model [18]. This is mainly due to the fact that Γ_δ, the second most significant contribution to Γ_{eff} after Γ_0, is 50% larger in the case of the BB model compared to the HC model. It should be noted that the Γ_{eff} and Δ_{eff} obtained from Eqs. (26a) and (26b), agree with the Γ_{exact} and Δ_{exact} obtained from the original SDBBP within X and Y %, respectively.

Figure 3 compares the SDBBP [6] with $\alpha = 2$, 1, 0 with Lorentz profiles derived from the BB model (LP^{BB}) and the HC model (LP^{HC}). It shows that LP$^{BB}(\alpha = 2)$ provides a good approximation of SDBBP($\alpha = 2$), with a difference of about 2% at the maximum of the profile. In contrast, LP^{HC} exhibits a much larger deviation. The LP^{HC} follows closely LP$^{BB}(\alpha = 1)$ and SDBBP($\alpha = 1$). The discrepancy between SDBBP($\alpha = 2$) and LP^{HC} is caused by the fact that, in the case of the HC model, the frequency of speed-changing collisions ν_{v^2} does not capture its dependence on α, which is about $2/3$ times smaller for the BB model with the same parameter values and $\alpha = 2$. On the other hand the frequency of speed-changing collisions ν_{v^2} for HC model agrees within 2% with those from BB model with $\alpha = 1$. A comparison of SDBBP($\alpha = 2$) with soft collision profiles LP^{SC} and SDGP [44] which are equivalent to LP$^{BB}(\alpha = 0)$ and SDBBP($\alpha = 0$), respectively, looks even worse. It is caused by the fact that the BB model with the same parameter values and $\alpha = 2$ has the frequency of speed-changing collisions ν_{v^2} only about $1/3$ of this in SC model (BB model with $\alpha = 0$).

VII. CONCLUSIONS

In summary, we demonstrated that under the limit of frequent velocity-changing collisions, the speed-dependent Dicke-narrowed profile of the spectral line collapses to the Lorentz profile. Our work provides formulas for effective Lorentzian width and shift, which take into account the arbitrary speed dependence of collisional broadening and shift, as well as the velocity-changing collision operator. Specifically, for the asymptotic behavior of the quadratic speed-dependent billiard ball profile [6], we obtained simple analytical expressions for Lorentzian width and shift. Our results generalize those recently reported in Ref. [18] for the speed-dependent hard collision profile [20] to the case of arbitrary perturber/absorber mass ratio, α. We verified the applicability of our formulas by comparing them with numerical calculations of quadratic speed-dependent billiard ball profiles over a wide range of line-shape parameters.

Finally, our comparison with the numerical calculation of the H_2 spectral line perturbed by He showed good agreement with the profile derived in this work. This is thanks to properly accounting for the perturber/absorber

mass ratio, which was not possible with the hard collision model. Our results offer a more accurate and general description of spectral line shapes under the limit of frequent velocity-changing collisions, with potential applications in various fields including atmospheric and astrophysical spectroscopy involving rovibrational transitions of molecular hydrogen.

Appendix A: The Burnett functions representation

For evaluation of the speed-dependent Dicke-narrowed spectral line shape from the transport/relaxation equation we use a subset of the Burnett functions having axial symmetry about the wave vector $\vec{k}$ [9]. A detailed discussion of the application of this set of basis functions, as well as matrix representation of the operators present in the transport/relaxation equation, can be found in Ref. [6]. For convenience we recall these results here, using the original formulation.

We assume the basis functions in the following form [10]:

$$\varphi_{nl}(\vec{v}) = N_{nl} (v/v_{m_A})^l L_n^{l+1/2}(v^2/v_{m_A}^2) P_l(\vec{e}_k \cdot \vec{e}_v), \quad \text{(A1)}$$

where a normalization factor,

$$N_{nl} = \sqrt{\frac{\pi^{1/2} n! (2l+1)}{2 \Gamma(n+l+3/2)}}, \quad \text{(A2)}$$

$\Gamma(...)$ is the gamma-Euler function. The associated Laguerre polynomials are defined as

$$L_n^{l+1/2}(x^2) = \sum_{m=0}^{n} \frac{(-1)^m \Gamma(n+l+3/2)}{m! (n-m)! \Gamma(m+l+3/2)} x^{2m}, \quad \text{(A3)}$$

where $x = v/v_{m_A}$ is the reduced speed of the active molecule. The Legendre polynomials are defined as

$$P_l(y) = \frac{1}{2^l} \sum_{k=0}^{[l/2]} \frac{(-1)^k (2l-2k)!}{k! (l-k)! (l-2k)!} y^{l-2k}, \quad \text{(A4)}$$

where $y = \vec{e}_k \cdot \vec{e}_v$ is the cosine of the angle between the velocity vector $\vec{v} = v\vec{e}_v$ and the wave vector $\vec{k} = k\vec{e}_k$, $\vec{e}_v$ and $\vec{e}_k$ are unit vectors.

The basis functions, $\varphi_{nl}(\vec{v})$, are eigenfunctions of the velocity-changing collision operator in the case of the soft collisions, where perturber/absorber mas ratio $\alpha = 0$. Like in [6], when calculating matrix elements of an operator, $\hat{A}$, we use the following notation $[\mathbf{A}]_{nl,n'l'} = (\varphi_{nl}(\vec{v}), \hat{A}\varphi_{n'l'}(\vec{v})) = \langle nl|\hat{A}|n'l'\rangle$.

The Doppler shift operator, $\vec{k} \cdot \vec{v} = \omega_D \vec{e}_k \cdot \vec{v}/v_{m_A}$, is represented by a matrix, $\mathbf{K}$, the elements of which are: [6]

$$[\mathbf{K}]_{nl,n'l'} = \omega_D \langle nl|\vec{e}_k \cdot \vec{v}/v_m|n'l'\rangle, \quad \text{(A5)}$$

where $\omega_D = kv_{m_A}$ and

$$\langle nl|\vec{e}_k \cdot \vec{v}/v_m|n'l'\rangle = \left[\sqrt{n+l+3/2}\, \delta_{n,n'} - \sqrt{n}\, \delta_{n,n'+1}\right]$$
$$\times \sqrt{\frac{(l+1)^2}{4(l+1)^2-1}}\, \delta_{l,l'-1}$$
$$+ \left[\sqrt{n+l+1/2}\, \delta_{n,n'} - \sqrt{n+1}\, \delta_{n,n'-1}\right]$$
$$\times \sqrt{\frac{l^2}{4l^2-1}}\, \delta_{l,l'+1}. \quad \text{(A6)}$$

The speed-dependent collisional width and shift operator, $\hat{S}_D^f = -\Gamma(v) - i\Delta(v)$, is represented by a matrix, $\mathbf{S}_D^f$, the elements of which are: [6, 24]

$$[\mathbf{S}_D^f]_{nl,n'l'} =$$
$$\frac{4}{\sqrt{\pi}(2l+1)} N_{nl} N_{n'l} \delta_{l,l'} \int_0^\infty dx\, e^{-x^2} x^{2l+2} \times$$
$$\times L_n^{l+1/2}(x^2) L_{n'}^{l+1/2}(x^2) [\Gamma(xv_{m_A}) + i\Delta(xv_{m_A})]. \quad \text{(A7)}$$

In the case of quadratic speed-dependent collisional broadening and shift [15],

$$\Gamma(v) + i\Delta(v) = \Gamma_0 + i\Delta_0 + (\Gamma_2 + i\Delta_2)\left(\frac{v^2}{v_m^2} - \frac{3}{2}\right), \quad \text{(A8)}$$

the matrix elements can be written as

$$[\mathbf{S}_D^f]_{nl,n'l'} = - [\Gamma_0 + i\Delta_0 - (\Gamma_2 + i\Delta_2)3/2]\, \delta_{n,n'}\delta_{l,l'}$$
$$- [\Gamma_2 + i\Delta_2] \langle nl|v^2/v_m^2|n'l'\rangle, \quad \text{(A9)}$$

where

$$\langle nl|v^2/v_m^2|n'l'\rangle =$$
$$\left[(2n+l+3/2)\,\delta_{n,n'} - \sqrt{(n+l+1/2)n}\,\delta_{n,n'+1}\right.$$
$$\left. - \sqrt{(n+l+3/2)(n+1)}\,\delta_{n,n'-1}\right]\delta_{l,l'}. \quad \text{(A10)}$$

The velocity-changing collisions operator $\hat{S}_{BB}^f$ in the billiard ball model is represented by a matrix, $\mathbf{S}_{BB}^f$, the elements of which are: [9, 10]

$$[\mathbf{S}_{BB}^f]_{nl,n'l'} = \nu^{(0)}\,M_{nl,n'l'}^{E*}, \quad \text{(A11)}$$

where $\nu^{(0)} = v_m^2/(2D^{(0)})$ and

$$D^{(0)} = \frac{3}{8}\left(\frac{k_B T}{2\pi\mu}\right)^{1/2}\frac{1}{N\sigma^2} \quad \text{(A12)}$$

is the first-order self-diffusion coefficient for rigid spheres, σ is the average of the rigid sphere diameter of the absorber and perturber, N is the number density of perturbers, $\mu = m_A m_P/(m_A + m_P)$ is the reduced mass. The analytical expressions for coefficients $M_{nl,n'l'}^{E*}$ for billiard ball model were derived by Lindenfeld and Shizgal [9, 10]

$$M_{nl,n'l'}^{E*} =$$
$$-\delta_{l,l'}\frac{3\,l!}{8M_2}\sqrt{\frac{n!\,n'!}{\Gamma(n+l+3/2)\Gamma(n'+l+3/2)}}\times$$
$$\left\{\sum_{p=0}^{\tilde{n}}\sum_{s=0}^{\tilde{n}-p}\sum_{m=0}^{\tilde{n}-p-s}\sum_{q=0}^{l}\sum_{r=0}^{l-q}\left[\frac{4^p\,(r+s+p+q+1)!}{(p+q+1)!\,r!\,s!}\right]\times\right.$$
$$\left[\frac{\Gamma(n+n'-2s-2p-m+l-r-q-1/2)\,B_{p,q}^{(1)}(\infty)}{(n-m-s-p)!\,(n'-m-s-p)!\,(l-r-q)!\,m!}\right]\times$$
$$\left.\left[M_1^{l+p-r-q}M_2^{n+n'+q-2m-2s-p}(M_1-M_2)^{m+r+2s}\right]\right\},$$
$$\text{(A13)}$$

where $M_1 = m_A/(m_A + m_P) = 1 - M_2$, $\tilde{n} = \min(n,n')$ and

$$B_{p,q}^{(1)}(\infty) = \frac{(2p+q+1)!}{2q!\,(2p+1)!} - \frac{2^{q-1}(p+q+1)!}{p!\,q!}\,. \quad \text{(A14)}$$

The exact diffusion coefficient D differs from $D^{(0)}$ and they are related by coefficient $f_D = D/D^{(0)}$ which evaluation is explained in Appendix B. Using these quantities the matrix elements can be written as

$$[\mathbf{S}_{BB}^f]_{nl,n'l'} = \nu_{\text{diff}}\,f_D\,M_{nl,n'l'}^{E*} \quad \text{(A15)}$$

where

$$\nu_{\text{diff}} = \frac{v_m^2}{2D} \quad \text{(A16)}$$

is the effective frequency of velocity-changing collisions.

Appendix B: Non-diagonal corrections to effective Lorentzian width and shift

Aiming at calculations of spectral line shape with quadratic speed-dependent collisional broadening and shift in the limit dominated by velocity-changing collisions, Eq. (5) can be rewritten in the Burnett functions representation,

$$1 = \left(-i(\omega - \omega_0) - [\mathbf{S}_D^f]_{00,00}\right)c_{00}(\omega)$$
$$+ i[\mathbf{K}]_{00,01}c_{01}(\omega) - [\mathbf{S}_D^f]_{00,10}c_{10}(\omega), \quad \text{(B1a)}$$

$$0 = i[\mathbf{K}]_{01,00}\delta_{n,0}c_{00}(\omega) - \sum_{n'=0}^{\infty}[\mathbf{S}_{VC}^f]_{n1,n'1}c_{n'1}(\omega), \quad \text{(B1b)}$$

$$0 = -[\mathbf{S}_D^f]_{10,00}\delta_{n,1}c_{00}(\omega) - \sum_{n'=1}^{\infty}[\mathbf{S}_{VC}^f]_{n0,n'0}c_{n'0}(\omega). \quad \text{(B1c)}$$

We also take advantage from the fact that $c_{00}(\omega)$ is not coupled to other coefficients by matrix $\mathbf{S}_{VC}^f$ and it dominates two other matrices $\mathbf{S}_D^f$ and $\mathbf{K}$. Therefore, in the limit of frequent velocity-changing collisions, we are allowed to use matrix $\mathbf{S}_{VC}^f$ and only those matrix elements of $\mathbf{S}_D^f$ and $\mathbf{K}$ which provide coupling of $c_{00}(\omega)$ to other coefficients in the transport/relaxation equation. With the velocity-changing collision operator in the form from Eq. (A11), we can find $c_{00}(\omega)$ by solving two other sets of linear equations,

$$\delta_{n,0} = -\sum_{n'=0}^{\infty}M_{n1,n'1}^{E*}a_{n'1}, \quad \text{(B2a)}$$

$$\delta_{n,1} = -\sum_{n'=1}^{\infty}M_{n0,n'0}^{E*}a_{n'0}. \quad \text{(B2b)}$$

Equations (B2a) and (B2b) are equivalent to Eqs. (B1b) and (B1c) when we set

$$c_{n1}(\omega) = -\frac{i[\mathbf{K}]_{01,00}}{\nu^{(0)}}c_{00}(\omega)a_{n1}, \quad \text{(B3a)}$$

$$c_{n0}(\omega) = \frac{[\mathbf{S}_D^f]_{10,00}}{\nu^{(0)}}c_{00}(\omega)a_{n0}. \quad \text{(B3b)}$$

Now we can rewrite Eq. (B1a) in the following form,

$$1 = \left(-i(\omega - \omega_0) - [\mathbf{S}_D^f]_{00,00}\right.$$
$$\left. + \frac{[\mathbf{K}]_{01,00}^2}{\nu^{(0)}}a_{01} - \frac{[\mathbf{S}_D^f]_{10,00}^2}{\nu^{(0)}}a_{10}.\right)c_{00}(\omega). \quad \text{(B4)}$$

It is convenient to introduce the coefficient $f_D = a_{01}(-M^{E*}_{01,01}) = a_{01}$, were a_{01} can be found by solving Eq. (B2a) [10]. Analogically, we can introduce $f_{v^2} = a_{10}(-M^{E*}_{10,10}) = a_{10}2/(1+\alpha)$, were a_{01} can be found by solving Eq. (B2b).

Table I collects the coefficients f_D and f_{v^2} as well as their ratios for the same set of α. We repeat the calculations of f_D performed by Lindenfeld in 1980 [10] for the billiard ball model but with higher numerical precision (our results are in good agreement for all but the last digit of the Table 1 of Ref.[10]). With these coefficients we define effective rates $\nu_{\vec{v}} = \nu^{(0)}/f_D$ of change of velocity vector $\vec{v}$ and $\nu_{v^2} = \nu^{(0)}(2/(1+\alpha))/f_{v^2}$ of change of v^2. From that we can obtain the relation $\nu_{v^2} = \nu_{\vec{v}}(2/(1+\alpha))(f_D/f_{v^2})$ between rates of change of $\vec{v}$ and v^2.

Solving Eq.(B4) yields

$$c_{00}(\omega) = \frac{1}{\Gamma_{\text{eff}} + i\Delta_{\text{eff}} - i(\omega - \omega_0)}, \qquad \text{(B5)}$$

where the effective Lorentzian width and shift are

$$\Gamma_{\text{eff}} + i\Delta_{\text{eff}} = -[\mathbf{S}^f_D]_{00,00} + \frac{[\mathbf{K}]^2_{01,00}}{\nu_{\vec{v}}} - \frac{[\mathbf{S}^f_D]^2_{10,00}}{\nu_{v^2}} . \quad \text{(B6)}$$

This equation can be also written in the following form,

$$\Gamma_{\text{eff}} + i\Delta_{\text{eff}} = \Gamma_0 + i\Delta_0 + \frac{1}{2}\frac{\omega_D}{\nu_{\vec{v}}} - \frac{3}{2}\frac{(\Gamma_2 + i\Delta_2)^2}{\nu_{\vec{v}}}\frac{1+\alpha}{2}\frac{f_{v^2}}{f_D}, \tag{B7}$$

which gives Eq. (25).

To take into account any arbitrary speed-dependence of collisional broadening, $\Gamma(v)$, and shift, $\Delta(v)$, we need to include other matrix elements, $[\mathbf{S}^f_D]_{n0,00}$, besides $[\mathbf{S}^f_D]_{10,00}$. In such case, Eqs. (B1a)-(B1b) should be generalized to the following form,

$$1 = \left(-i(\omega - \omega_0) - [\mathbf{S}^f_D]_{00,00}\right) c_{00}(\omega)$$
$$+ i[\mathbf{K}]_{00,01}c_{01}(\omega) - \sum_{n'=1}^{\infty}[\mathbf{S}^f_D]_{00,n'0}c_{n'0}(\omega), \quad \text{(B8a)}$$

$$0 = i[\mathbf{K}]_{01,00}\delta_{n,0}c_{00}(\omega) - \sum_{n'=0}^{\infty}[\mathbf{S}^f_{VC}]_{n1,n'1}c_{n'1}(\omega), \quad \text{(B8b)}$$

$$0 = -[\mathbf{S}^f_D]_{n0,00}c_{00}(\omega) - \sum_{n'=1}^{\infty}[\mathbf{S}^f_{VC}]_{n0,n'0}c_{n'0}(\omega). \quad \text{(B8c)}$$

The coefficient $c_{00}(\omega)$ can be found in analogical way like in Eqs. (B1a)-(B1b). The only difference is that the set of linear equations, Eq. (B2b), is replaced by

$$\frac{[\mathbf{S}^f_D]_{n0,00}}{\sum_{n'=1}^{\infty}[\mathbf{S}^f_D]_{n'0,00}} = -\sum_{n'=1}^{\infty}M^{E*}_{n0,n'0}a_{n'0}, \qquad \text{(B9)}$$

and scaling Eq. (B3b) is replaced by

$$c_{n0}(\omega) = \frac{\sum_{n'=1}^{\infty}[\mathbf{S}^f_D]_{n'0,00}}{\nu^{(0)}}c_{00}(\omega)a_{n0}. \qquad \text{(B10)}$$

Now from Eq. (B8a) we get

$$1 = \left(-i(\omega - \omega_0) - [\mathbf{S}^f_D]_{00,00} + \frac{[\mathbf{K}]^2_{01,00}}{\nu^{(0)}}a_{01}\right.$$
$$\left. - \frac{1}{\nu^{(0)}}\sum_{n=1}^{\infty}[\mathbf{S}^f_D]_{n0,00}\sum_{n'=1}^{\infty}[\mathbf{S}^f_D]_{n'0,00}a_{n'0}\right)c_{00}(\omega), \quad \text{(B11)}$$

and, as a consequence, the effective Lorentzian width and shift:

$$\Gamma_{\text{eff}} + i\Delta_{\text{eff}} = -[\mathbf{S}^f_D]_{00,00} + \frac{[\mathbf{K}]^2_{01,00}}{\nu_{\vec{v}}}$$
$$- \frac{1}{\nu^{(0)}}\sum_{n=1}^{\infty}[\mathbf{S}^f_D]_{n0,00}\sum_{n'=1}^{\infty}[\mathbf{S}^f_D]_{n'0,00}a_{n'0}. \quad \text{(B12)}$$

[1] J.-M. Hartmann, C. Boulet, and D. Robert, *Collisional Effects on Molecular Spectra: Laboratory Experiments and Model, Consequences for Applications* (Elsevier, Amsterdam, 2008).

[2] P. R. Berman, Speed-dependent collisional width and shift parameters in spectral profiles, J. Quant. Spectrosc. Radiat. Transfer **12**, 1331 (1972).

[3] J. Ward, J. Cooper, and E. W. Smith, Correlation effects in the theory of combined Doppler and pressure broadening – I. Classical theory, J. Quant. Spectrosc. Radiat. Transfer **14**, 555 (1974).

[4] R. H. Dicke, The effect of collisions upon the Doppler width of spectral lines, Phys. Rev. **89**, 472 (1953).

[5] J. P. Wittke and R. H. Dicke, Redetermination of the Hyperfine Splitting in the Ground State of Atomic Hydrogen, Phys. Rev. **103**, 620 (1956).

[6] R. Ciuryło, D. A. Shapiro, J. R. Drummond, and A. D. May, Solving the line-shape problem with speed-dependent broadening and shifting and with Dicke narrowing. II. Application, Phys. Rev. A **65**, 012502 (2002).

[7] H. M. Pickett, Effects of velocity averaging on the shapes of absorption lines, J. Chem. Phys. **73**, 6090 (1980).

[8] R. L. Farrow, L. A. Rahn, G. O. Sitz, and G. J. Rosasco, Observation of a speed-dependent collisional inhomogeneity in H$_2$ vibrational line profiles, Phys. Rev. Lett. **63**, 746 (1989).

[9] M. J. Lindenfeld and B. Shizgal, Matrix elements of the Boltzmann collision operator for gas mixtures, Chem.

Phys. **41**, 81 (1979).

[10] M. J. Lindenfeld, Self-structure factor of hard-sphere gases for arbitrary ratio of bath to test particle masses, J. Chem. Phys. **73**, 5817 (1980).

[11] P. N. M. Hoang, P. Joubert, and D. Robert, Speed-dependent line-shape models analysis from molecular dynamics simulations: The collision regime, Phys. Rev. A **65**, 012507 (2002).

[12] R. Ciuryło, D. Lisak, and J. Szudy, Role of velocity- and speed-changing collisions on speed-dependent line shapes of H_2, Phys. Rev. A **66**, 032701 (2002).

[13] P. Wcisło, I. E. Gordon, H. Tran, Y. Tan, S.-M. Hu, A. Campargue, S. Kassi, D. Romanini, C. Hill, R. V. Kochanov, and L. S. Rothman, The implementation of non-Voigt line profiles in the HITRAN database: H_2 case study, J. Quant. Spectrosc. Radiat. Transfer **177**, 75 (2016).

[14] R. Z. Martínez, D. Bermejo, F. Thibault, and P. Wcisło, Testing the ab initio quantum-scattering calculations for the D_2-He benchmark system with stimulated Raman spectroscopy, J. Raman Spectrosc. **49**, 1339 (2018).

[15] F. Rohart, H. Mäder, and H.-W. Nicolaisen, Speed dependence of rotational relaxation induced by foreign gas collisions: Studies on CH_3F by millimeter wave coherent transients, J. Chem. Phys. **101**, 6475 (1994).

[16] M. Nelkin and A. Ghatak, Simple Binary Collision Model for Van Hove's $G_s(r, \ t)$, Phys. Rev. **135**, A4 (1964).

[17] S. G. Rautian and I. I. Sobelman, The effect of collisions on the Doppler broadening of spectral lines, Usp. Fiz. Nauk **90**, 209 (1966) [Sov. Phys. Usp. **9**, 701 (1967)].

[18] N. Stolarczyk, P. Wcisło, and R. Ciuryło, Inhomogeneous broadening, narrowing and shift of molecular lines under frequent velocity-changing collisions, J. Quant. Spectrosc. Radiat. Transfer **287**, 108246 (2022).

[19] B. Lance, G. Blanquet, J. Walrand, and J.-P. Bouanich, On the Speed-Dependent Hard Collision Lineshape Models: Application to C_2H_2 Perturbed by Xe, J. Mol. Spectrosc. **185**, 262 (1997).

[20] A. S. Pine, Asymmetries and correlations in speed-dependent Dicke-narrowed line shapes of argon-broadened HF, J. Quant. Spectrosc. Radiat. Transfer **62**, 397 (1999).

[21] R. Blackmore, A modified Boltzmann kinetic equation for line shape functions, J. Chem. Phys. **87**, 791 (1987).

[22] D. A. Shapiro, R. Ciuryło, J. R. Drummond, and A. D. May, Solving the line-shape problem with speed-dependent broadening and shifting and with Dicke narrowing. I. Formalism, Phys. Rev. A **65**, 012501 (2002).

[23] E. V. Podivilov, A. I. Chernykh, and D. A. Shapiro, Ion line narrowing in a dense plasma, J. Exp. Theo. Phys. **78**, 653 (1994).

[24] D. Robert and L. Bonamy, Memory effects in speed-changing collisions and their consequences for spectral lineshape: I. collision regime, Eur. Phys. J. D **2**, 245 (1998).

[25] R. Ciuryło, A. Bielski, J. R. Drummond, D. Lisak, A. D. May, A. S. Pine, D. A. Shapiro, S. J., and R. S. Trawński, High-resolution studies on the influence of velocity-changing collisions on atomic and molecular line shapes, in *Spectral Line Shapes*, Vol. 12, edited by C. A. Back (American Institute of Physics, New York, 2002) pp. 151–160.

[26] R. Wehr, A. Vitcu, R. Ciuryło, F. Thibault, J. R. Drummond, and A. D. May, Spectral line shape of the P(2) transition in CO-Ar: Uncorrelated *ab initio* calculation, Phys. Rev. A **66**, 062502 (2002).

[27] P. Wcisło, F. Thibault, M. Zaborowski, S. Wójtewicz, A. Cygan, G. Kowzan, P. Masłowski, J. Komasa, M. Puchalski, K. Pachucki, R. Ciuryło, and D. Lisak, Accurate deuterium spectroscopy for fundamental studies, J. Quant. Spectrosc. Radiat. Transfer **213**, 41 (2018).

[28] M. Słowiński, F. Thibault, Y. Tan, J. Wang, A.-W. Liu, S.-M. Hu, S. Kassi, A. Campargue, M. Konefał, H. Jóźwiak, K. Patkowski, P. Żuchowski, R. Ciuryło, D. Lisak, and P. Wcisło, H_2-He collisions: *Ab initio* theory meets cavity-enhanced spectra, Phys. Rev. A **101**, 052705 (2020).

[29] S. Dolbeau, R. Berman, J. R. Drummond, and A. D. May, Dicke narrowing as an example of line mixing, Phys. Rev. A **59**, 3506 (1999).

[30] D. A. Shapiro and A. D. May, Dicke narrowing for rigid spheres of arbitrary mass ratio, Phys. Rev. A **63**, 012701 (2001).

[31] A. Pine, Line shape asymmetries in Ar-broadened HF(v=1–0) in the Dicke-narrowing regime, Chem. Phys. **101**, 3444 (1994).

[32] L. Demeio, S. Green, and L. Monchick, Effects of velocity changing collisions on line shapes of HF in Ar, J. Chem. Phys. **102**, 9160 (1995).

[33] G. Nienhuis, Effects of the radiator motion in the classical and quantum-mechanical theories of collisional spectral-line broadening, J. Quant. Spectrosc. Radiat. Transfer **20**, 275 (1978).

[34] J. P. Loony, *Comprehensive theory for the broadening, shifting and narrowing of HF and HCl fundamental band absorption profiles*, Ph.D. thesis, Department of Physics, The Pennsylvania State University, University Park, PA, USA (1987).

[35] R. Ciuryło, A. S. Pine, and J. Szudy, A generalized speed-dependent line profile combining soft and hard partially correlated Dicke-narrowing collisions, J. Quant. Spectrosc. Radiat. Transfer **68**, 257 (2001).

[36] S. Hess, Kinetic theory of spectral line shapes. The transition between Doppler broadening and collisional broadening, Physica **61**, 80 (1972).

[37] V. P. Kochanov, S. G. Rautian, and A. M. Shalagin, Broadening of nonlinear resonances by velocity-changing collisions, Zh. Eksp. Teor. Fiz. **72**, 1358 (1977) [Sov. Phys. JETP **45**, 714 (1977)].

[38] P. R. Berman, T. W. Mossberg, and S. R. Hartmann, Collision kernels and laser spectroscopy, Phys. Rev. A **25**, 2550 (1982).

[39] P. R. Berman, Collisions in atomic vapors, in *Les Houches, Session XXXVIII, 1982 – Tendances actuelles en physique atomique / New trends in atomic physics*, Vol. I, edited by G. Grynberg and R. Stora (Elsevier Science Publisher, Amsterdam, 1984) pp. 451–514.

[40] L. Monchick and L. W. Hunter, Diatomic–diatomic molecular collision integrals for pressure broadening and Dicke narrowing: A generalization of Hess's theory, The Journal of Chemical Physics **85**, 713 (1986), https://pubs.aip.org/aip/jcp/article-pdf/85/2/713/9724657/713_1_online.pdf.

[41] F. Thibault, K. Patkowski, P. S. Żuchowski, H. Jóźwiak, R. Ciuryło, and P. Wcisło, Rovibrational line-shape parameters for H_2 in He and new H_2-He potential energy surface, Journal of Quantitative Spectroscopy and Radiative Transfer **202**, 308 (2017).

[42] S. Chandrasekhar, Stochastic problems in physics and astronomy, Rev. Mod. Phys. **15**, 1 (1943).

[43] L. Galatry, Simultaneous effect of Doppler and foreign gas broadening on spectral lines, Phys. Rev. **122**, 1218 (1961).

[44] R. Ciuryło, R. Jaworski, J. Jurkowski, A. S. Pine, and J. Szudy, Spectral line shapes modeled by a quadratic speed-dependent Galatry profile, Phys. Rev. A **63**, 032507 (2001).

[45] D. Priem, F. Rohart, J.-M. Colmont, G. Wlodarczak, and J.-P. Bouanich, Lineshape study of the J=3←2 rotational transition of CO perturbed by N_2 and O_2, J. Mol. Struct. **517-518**, 435 (2000).

[46] R. Ciuryło and R. Szudy, Speed-dependent pressure broadening and shift in the soft collision approximation, J. Quant. Spectrosc. Radiat. Transfer **57**, 411 (1997).

[47] P. Wcisło, H. Tran, S. Kassi, A. Campargue, F. Thibault, and R. Ciuryło, Velocity-changing collisions in pure H_2 and H_2-Ar mixture, J. Chem. Phys. **141**, 074301 (2014).

[48] D. Lisak, J. T. Hodges, and R. Ciuryło, Comparison of semiclassical line-shape models to rovibrational H_2O spectra measured by frequency-stabilized cavity ring-down spectroscopy, Phys. Rev. A **73**, 012507 (2006).

[49] P. Wcisło, F. Thibault, H. Cybulski, and R. Ciuryło, Strong competition between velocity-changing and phase- or state-changing collisions in h$_2$ spectra perturbed by ar, Phys. Rev. A **91**, 052505 (2015).

[50] P. Wcisło, F. Thibault, N. Stolarczyk, H. Jóźwiak, M. Słowiński, M. Gancewski, K. Stankiewicz, M. Konefał, S. Kassi, A. Campargue, Y. Tan, J. Wang, K. Patkowski, R. Ciuryło, D. Lisak, R. Kochanov, L. Rothman, and I. Gordon, The first comprehensive dataset of beyond-Voigt line-shape parameters from ab initio quantum scattering calculations for the HITRAN database: He-perturbed H_2 case study, J. Quant. Spectrosc. Radiat. Transfer **260**, 107477 (2021).

[51] M. Słowiński, H. Jóźwiak, M. Gancewski, K. Stankiewicz, N. Stolarczyk, Y. Tan, J. Wang, A.-W. Liu, S.-M. Hu, S. Kassi, A. Campargue, K. Patkowski, P. S. Żuchowski, R. Ciuryło, F. Thibault, and P. Wcisło, Collisional line-shape effects in accurate He-perturbed H_2 spectra, Journal of Quantitative Spectroscopy and Radiative Transfer **277**, 107951 (2022).